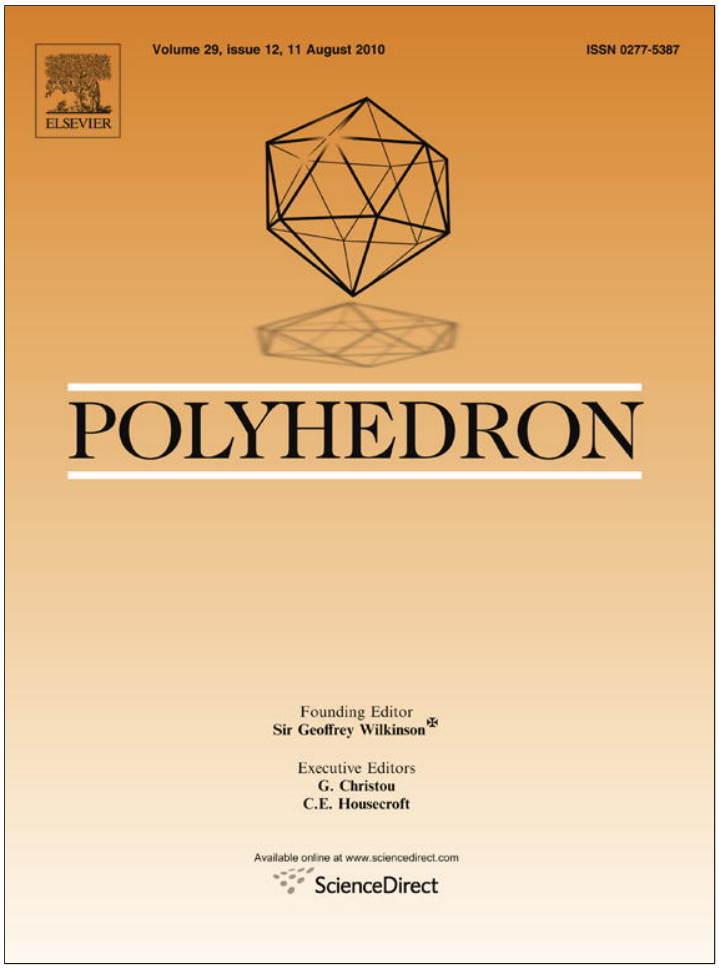

Polyhedron 29 (2010) 2537–2545

Contents lists available at ScienceDirect

Polyhedron

journal homepage: www.elsevier.com/locate/poly

Iron, copper and zinc ammonium-1-hydroxyalkylidene-diphosphonates with zero-, one- and two-dimensional covalent metal–ligand structures extended into three-dimensional supramolecular networks by charge-assisted hydrogen-bonding

Hesham A. Habib [a], Beatriz Gil-Hernández [b], Khalid Abu-Shandi [a,c], Joaquín Sanchiz [b], Christoph Janiak [a,*]

[a] Institut für Anorganische und Analytische Chemie, Universität Freiburg, Albertstr. 21, D-79104 Freiburg, Germany
[b] Departamento de Química Inorganíca, Universidad de La Laguna, 38206 La Laguna, Tenerife, Spain
[c] Department of Chemistry, Tafila Technical University, P.O. Box 179, Tafila 66110, Jordan

ARTICLE INFO

Article history:
Received 2 February 2010
Accepted 27 May 2010
Available online 31 May 2010

Keywords:
Bisphosphonate
Diphosphonate
Iron
Copper
Zinc
Magnetism
Polarography

ABSTRACT

Hydrothermal synthesis with MCl_2 (M = Fe, Cu, and Zn) and disodium 5-ammonium-1-hydroxypentylidene-1,1-bisphosphonate, $(Na^+)_2[^+H_3N(CH_2)_4C(OH)(PO_3^{2-})(PO_3H^-)]$ ($Na_2HAC_5OHP_2$) or sodium 3-ammonium-1-hydroxypropylidene-1,1-bisphosphonate hydrate, $Na^+[^+H_3N(CH_2)_2C(OH)(PO_3H^-)(PO_3H^-)]\cdot H_2O$ ($NaH_2PAM\cdot H_2O$) the sodium salt of pamidronic acid, H_3PAM) yielded the one-dimensional (1D) iron, molecular copper and two-dimensional (2D) zinc compounds 1D-{[$Fe(\mu_3\text{-}\eta^5\text{-}HAC_5OHP_2)]\cdot H_2O$}, **1**, [$Cu(\eta^2\text{-}H_2AC_5OHP_2)_2$], **2**, 2D-{[$Zn_2(\mu_5\text{-}\eta^7\text{-}AC_5OHP_2)Cl$], **3**, and 2D-{[$Zn(\mu_2\text{-}\eta^3\text{-}H_2PAM)_2$], **4**, respectively. The bisphosphonate ligand bridges (μ_n) between **2**–**5** metal atoms and uses **2**–**7** oxygen donor atoms towards metal coordination (η^n). The zwitterionic nature of the now bis- or tetrakis-deprotonated ammonium–bisphosphonate is retained in the metal complexes. From the reaction of $NiCl_2$ and $Na_2HAC_5OHP_2$ the zwitterionic 5-ammonium-1-hydroxypentylidene-1-phosphonic acid, $^+H_3N(CH_2)_4CH(OH)PO_3H^-$, **5** was obtained as a product of the ligand P–C bond hydrolysis. Adjacent strands, molecules or layers in **1**–**4**, respectively are organized through the Coulomb attraction between the positive ammonium group and the negative phosphonate groups, supported by hydrogen-bonding. Each protic H atom on the C–OH, NH_3^+ and $-PO_3H^-$ group is involved in charge-assisted hydrogen-bonding. The ammonium-pentylidene groups act as hydrophobic separators between the hydrophilic units with the polar M{$C(OH)(PO_3)_2$} and {NH_3} units. Bond valence sum calculations support the Fe(II) oxidation state in **1**, which was experimentally determined from a quantitative polarographic Fe(II)/Fe(III) speciation analysis as well as a temperature variable magnetic study.

1. Introduction

Metal (organo)phosphonates and organo-di- or bisphosphonates offer potential applications in catalysis, ion exchange, proton conduction, absorption, molecular recognition, separation and sensors [1–6]. Cobalt, iron and other (di/bis)phosphonates are also investigated for their magnetic properties [7–10]. Organo(di/bis)phosphonates (Scheme 1) can contain additional functional groups such as carboxylate, hydroxyl or amino in the organo-moiety which presents a tunable functionality with a wide variety of structural motifs and properties [11]. Diphosphonates play a role in biological systems, including the removal of iron from iron proteins [12]. The compound 3-ammonium-1-hydroxypropylidene-1,1-bisphosphonate (=pamidronate, Scheme 1) as the disodium salt is used clinically in the diagnosis and treatment of diseases affecting bone tissue [13–16], zoledronic acid for treatment of postmenopausal osteoporosis [17]. Metal organophosphonates are an extensive class of organic–inorganic hybrid materials with a wide variety of structural motifs including clusters, layers and networks. Following a report on Fe(II)-pamidronate, 2D-[$Fe^{II}\{H_2PAM\}_2$] [18] and mixed-valence Fe(II/III)-5-ammonium-1-hydroxypentylidene-1,1-bisphosphonate, 2D-[$\{Fe^{II/III}(H_2O)_2\}\{Fe^{III/II}Cl\}_2(\mu_4\text{-}AC_5OHP_2)_2]\cdot 4H_2O$ [19] we describe here on the synthesis and structural characterization of iron, copper and zinc complexes of $H_{3-n}AC_5OHP_2^{n-}$ and a zinc complex of H_2PAM^- (Scheme 1).

2. Experimental

2.1. Physical measurements and materials

IR spectra were recorded in the range 400–4000 cm^{-1} on a Bruker Optik IFS 25 (KBr pellet) or on a Nicolet Magna-IR 760

* Corresponding author. Tel.: +49 761 2036127.
E-mail address: janiak@uni-freiburg.de (C. Janiak).

0277-5387/$ - see front matter © 2010 Elsevier Ltd. All rights reserved.
doi:10.1016/j.poly.2010.05.025

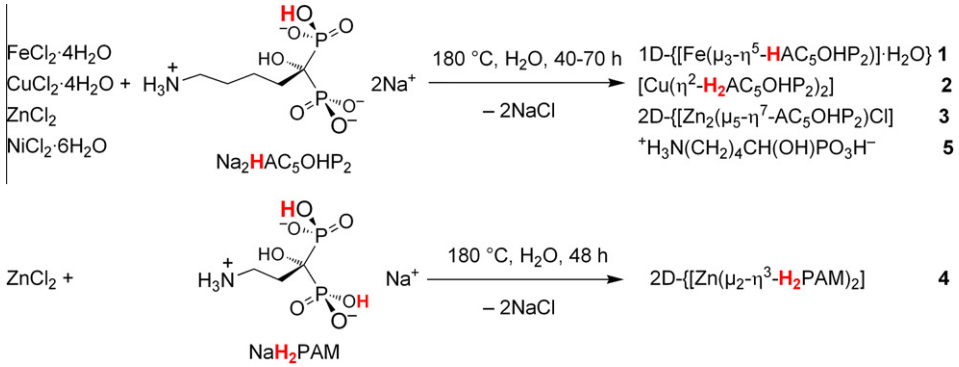

Scheme 1. Synthetic scheme for **1**–**5**. The notation μ_n indicates the ligand bridging action between n metal atoms and η^n the number (n) of oxygen donor atoms used by the ligand towards metal coordination.

Fourier-transform spectrometer using a diamond orbit ATR (ATR = attenuated total reflection) unit. Elemental analyses were obtained on a VarioEL from Elementaranalysensysteme GmbH. X-ray powder diffractometry was done on a Stoe STADI P with Debye–Scherrer geometry, Mo Kα radiation ($\lambda = 0.7093$ Å) and a Ge(1 1 1) monochromator and the samples in glass capillaries on a rotating probe head. Polarographic iron measurements for the iron percentage and oxidation state were carried out using a multi-mode dropping mercury electrode in differential pulse mode on a Metrohm 797 VA Computrace in the voltage region from −1.4 to −0.1 V [20]. The measurements were done in a degassed 0.1 mol/L sodium pyrophosphate solution. Solutions used for the polarographic measurements were degassed by bubbling gaseous nitrogen (5.0–99.999 purity) for 15 min through the solution. The standard addition method was used to quantitatively determine the amount of iron(II) and iron(III) in the sample. Ammonium iron(III) sulfate decahydrate was used for the preparation of the iron(III) standard. Ammonium iron(II) sulfate hexahydrate was used as the iron(II) standard. The standard concentrations were adjusted to the sample concentration.

Magnetic susceptibility measurements on polycrystalline samples were carried out in the temperature range 1.9–100 K by means of a Quantum Design SQUID magnetometer operating at 1000 Oe ($T < 15$ K) and 10,000 Oe ($T > 15$ K). Diamagnetic corrections of the constituent atoms were estimated from Pascal's constants and experimental susceptibilities were also corrected for the magnetization of the sample holder.

The compound disodium (5-ammonium-1-hydroxypentylidene-1,1-bisphosphonate) (=5-amino-1-hydroxypentylidene-1,1-bisphosphonic acid disodium salt), $Na_2[H_3N(CH_2)_4C(OH)(PO_3)(PO_3H)]$ ($Na_2HAC_5OHP_2$) (M = 307.09 g/mol), and the sodium salt of pamidronate, sodium (3-ammonium-1-hydroxypropylidene-1,1-biphosphonate) monohydrate (=3-amino-1-hydroxypropylidene-1,1-bisphosphonic acid monosodium salt), $Na[H_3N(CH_2)_2C(OH)(PO_3H)(PO_3H)]\cdot H_2O$ ($NaH_2PAM\cdot H_2O$) (M = 275.07 g/mol), were prepared by the method of Kieczykowski and coworkers [21].

2.2. Preparations

2.2.1. catena-{μ_3-(5-ammonium-1-hydroxypentylidene-1,1-bisphosphonato-κO:O′,O‴:O′ᵛ,Oᵛ′)iron(II)}, 1D-{[Fe(μ_3-η^5-HAC$_5$OHP$_2$)]·H$_2$O} (**1**)

A mixture of $FeCl_2\cdot 4H_2O$ (199 mg, 1.00 mmol), $Na_2HAC_5OHP_2$ (312 mg, 1.02 mmol) and water (10 mL) was stirred for 30 min at room temperature, transferred to a Teflon-lined stainless-steel autoclave and heated at 180 °C for 50 h. Then the autoclave was cooled to room temperature at a rate of 5 °C h^{-1}. An orange-yellow crystalline product was filtered off, washed with distilled water and dried in air. Yield 136 mg, 41%. IR (ATR): 3248 (w), 3180 (w), 3006 (w), 1162 (m), 1492 (m), 1495 (w), 1407 (w), 1317 (w), 1162 (w), 1048 (s), 999 (s), 953 (s), 922 (s), 897 (m), 876 (m), 768 (m), 697 (m), 611 (m), 586 (m), 531 (m), 475 (m), 444 (m) cm^{-1}. *Anal.* Calc. for $C_5H_{15}FeNO_8P_2$ (334.97): C, 17.93; H, 4.51; N, 4.18; Fe, 16.67. Found: C, 17.54; H, 4.66; N, 4.23; Fe, 15.6%.

For the polarographic iron content and oxidation state analysis 10 mg of product was dissolved in 10 mL of desoxygenated (50% v/v) H_2SO_4/H_2O solution. From this solution 0.10 mL was added into 20.0 mL of the sodium pyrophosphate solution in the polarographic cell (dilution by a factor of 201). An iron(II) concentration of (0.156 ± 0.004) mg/mL and a small iron(III) concentration was determined (Fig. S7) corresponding to an Fe(II) percentage of 15.6% (Fig. S8, Supplementary data).

2.2.2. Bis(5-ammonium-1-hydroxypentylidene-1,1-bisphosphonato-κO,O‴)copper(II), [Cu(η^2-H$_2$AC$_5$OHP$_2$)$_2$], (**2**)

A mixture of $CuCl_2\cdot 2H_2O$ (170 mg, 1.00 mmol), $Na_2HAC_5OHP_2$ (624 mg, 2.04 mmol) and water (10 mL) was stirred for 30 min at room temperature, transferred to a Teflon-lined stainless-steel autoclave and heated at 180 °C for 40 h. Then the autoclave was cooled to room temperature at a rate of 10 °C h^{-1}. A green crystalline product was filtered off, washed with distilled water and dried in air. Yield 175 mg, 30%. IR (KBr): 3377 (m), 3268 (w), 3110 (m), 2973 (w), 1623 (s), 1521 (m), 1482 (m), 1319 (m), 1297 (w), 1149 (m), 1081 (m), 1013 (m), 935 (m), 838 (m), 772 (m), 728 (m), 670 (m), 607 (m), 571 (s), 500 (m), 471 (m) cm^{-1}. *Anal.* Calc. for $C_{10}H_{24}CuN_2O_{14}P_4$ (583.74): C, 20.58; H, 4.14; N, 4.80. Found: C, 18.88; H, 4.47; N, 4.32%.

2.2.3. Catena-{μ_5-(5-ammonium-1-hydroxypentylidene-1,1-bisphosphonato-κO:O′:O″,O‴:O′ᵛ:Oᵛ,Oᵛ′)-chloro-dizinc(II)}, 2D-{[Zn$_2$(μ_5-η^7-AC$_5$OHP$_2$)Cl] (**3**)

A mixture of $ZnCl_2$ (136 mg, 1.00 mmol), $Na_2HAC_5OHP_2$ (624 mg, 2.04 mmol) and water (10 mL) was stirred for 30 min. at room temperature, transferred to a Teflon-lined stainless-steel autoclave and heated at 180 °C for 40 h. Then the autoclave was cooled to room temperature at a rate of 10 °C h^{-1}. A colorless crystalline product was filtered off, washed with distilled water and dried in air. Yield 155 mg, 70% based on Zn. IR (KBr): 3546 (m), 3340 (m), 3066 (m), 2950 (w), 1601 (m), 1505 (m), 1355 (w), 1322 (w), 1094 (s), 1017 (s), 964 (m), 930 (w), 843 (m), 739 (m), 672 (m), 586 (s), 474 (m), 424 (w) cm^{-1}. *Anal.* Calc. for $C_5H_{14}Zn_2NO_8P_2Cl$ (444.32): C, 13.52; H, 3.18; N, 3.15. Found: C, 13.71; H, 3.22; N, 3.22%.

2.2.4. Catena-{bis-μ-(5-ammonium-1-hydroxypropylidene-1,1-bisphosphonato-κO,O‴:Oᵛ)zinc(II)}, catena-{bis-μ-(pamidronato)zinc(II)}, 2D-{[Zn(μ_2-η^3-H$_2$PAM)$_2$] (**4**)

A mixture of $ZnCl_2$ (68 mg, 0.5 mmol), $NaH_2PAM\cdot H_2O$ (284 mg, 1.03 mmol) and water (10 mL) was stirred for 30 min at room

Table 1
Crystal data and structure refinement for **1**-**5**.

Compound	**1**	**2**	**3**	**4**	**5**
Empirical formula	$C_5H_{15}FeNO_8P_2$	$C_{20}H_{56}Cu_2N_4O_{28}P_8$ [e]	$C_5H_{14}ClNO_8P_2Zn_2$	$C_6H_{20}N_2O_{14}P_4Zn$	$C_5H_{14}NO_4P$
M (g mol^{-1})	334.97	1175.53	444.34	533.49	183.14
Crystal size (mm)	0.60 × 0.06 × 0.03	0.15 × 0.11 × 0.08	0.25 × 0.22 × 0.03	0.35 × 0.33 × 0.03	0.23 × 0.22 × 0.15
Crystal appearance	needle, yellow	isometric, green	plate, colorless	plate, colorless	isometric, colorless
2θ range (°)	8.10–53.70	3.78–50.30	4.12–53.90	4.30–52.70	4.26–50.70
h; k; l range	−7, 5; ±17; ±18	−11, 10; ±12; ±14	±10; ±10; ±13	±47; ±8; ±16	±11; ±6; −20, 19
Crystal system	triclinic	triclinic	triclinic	monoclinic	monoclinic
Space group	$P\bar{1}$	$P\bar{1}$	$P\bar{1}$	$C2/c$	$P2_1/c$
a (Å)	5.5204(3)	9.5037(5)	8.1805(3)	37.9560(8)	9.5594(3)
b (Å)	14.0381(7)	10.1084(6)	8.3881(4)	6.7259(2)	5.3926(2)
c (Å)	14.2388(7)	11.9048(7)	10.3572(4)	12.9474(3)	16.7813(5)
α (°)	90.726(3)	73.260(3)	75.270(2)	90	90
β (°)	95.356(3)	70.234(3)	77.932(2)	91.036(2)	90.800(2)
γ (°)	94.292(3)	83.996(3)	76.967(2)	90	90
V (Å^3)	1095.34(10)	1030.63(10)	660.90(5)	3304.78(14)	864.99(5)
Z	4	1	2	8	4
D_{calc} (g cm^{-3})	2.031	1.894	2.233	2.144	1.406
F(0 0 0)	688	606	444	2176	392
μ (mm^{-1})	1.700	1.445	4.105	1.955	0.289
Maximum/minimum transmission	0.9508/0.4285	0.8932/0.8124	0.8868/0.4268	0.9437/0.5478	0.9579/0.9364
Reflections collected	9759	17,593	16,827	24,939	15,428
Independent reflections	4540(0.0345)	3633(0.0510)	2866(0.0330)	3365 (R_{int} = 0.0529)	1582 (R_{int} = 0.0332)
Observed reflections [$I > 2(I)$]	3702	3137	2592	2857	1386
Parameters refined	349	280	190	280	115
Maximum/minimum $\Delta\rho$[a] (e Å^{-3})	0.477/−0.411	2.171/−0.803[f]	0.442/−0.393	0.545/−0.360	0.371/−0.285
R_1/wR_2 [$I > 2(I)$] [b]	0.0314/0.0731	0.0691/0.1791	0.0193/0.0464	0.0273/0.0630	0.0365/0.0902
R_1/wR_2 (all reflections) [b]	0.0428/0.0782	0.0776/0.1827	0.0232/0.0479	0.0362/0.0663	0.0425/0.0936
Goodness-of-fit (GOF) on F^2[c]	1.041	1.099	1.061	1.040	1.063
Weight scheme w; a/b[d]	0.0367/0.0521	0.0450/22.5665	0.0227/0.4330	0.0323/5.4693	0.0420/0.7023

[a] Largest difference peak and hole.
[b] $R_1 = [\sum(||F_o| - |F_c||)/\sum|F_o|]$; $wR_2 = [\sum[w(F_o^2 - F_c^2)^2]/\sum[w(F_o^2)^2]]^{1/2}$.
[c] Goodness-of-fit = $[\sum[w(F_o^2 - F_c^2)^2]/(n-p)]^{1/2}$.
[d] $w = 1/[^2(F_o^2) + (aP)^2 + bP]$ where $P = (\max(F_o^2 \text{ or } 0) + 2F_c^2)/3$.
[e] Doubled molecular formula of the dimeric unit as suggested by checkcif.
[f] Largest residual electron density in the vicinity of the two N atoms.

temperature, transferred to a Teflon-lined stainless-steel autoclave and heated at 180 °C for 48 h. Then the autoclave was cooled to room temperature at a rate of 5 °C h^{-1}. A colorless crystalline product was filtered off, washed with distilled water and dried in air. Yield 120 mg, 45%. IR (KBr): 3350 (w), 3290 (w), 3245 (w), 3181 (w), 3015 (w), 2889 (w), 1618 (m), 1471 (s), 1388 (w), 1309 (m), 1148 (s), 1072 (s), 999 (m), 958 (m), 916 (m), 872 (m), 768 (w), 664 (m), 584 (s), 533 (s), 492 (s), 433 (s) cm^{-1}. *Anal.* Calc. for $C_6H_{20}ZnN_2O_{14}P_4$ (533.49): C, 13.51; H, 3.78; N, 5.25. Found: C, 13.59; H, 3.82; N, 5.21%.

2.2.5. 5-Ammonium-1-hydroxypentylidene-1-phosphonic acid, $^+H_3N(CH_2)_4CH(OH)PO_3H^-$ (**5**)

A mixture of $NiCl_2{\cdot}6H_2O$ (238 mg, 1.00 mmol), $Na_2HAC_5OHP_2$ (1.248 g, 4.06 mmol) and water (10 mL) was stirred for 30 min at room temperature, transferred to a Teflon-lined stainless-steel autoclave and heated at 180 °C for 70 h. Then the autoclave was cooled to room temperature at a rate of 3.6 °C h^{-1}. A very light green square crystalline product was filtered off, washed with distilled water and dried in air. Yield 210 mg, 28%. *Anal.* Calc. for $C_5H_{14}NO_4P$ (183.14): C, 32.79; H, 7.71; N, 7.65. Found: C, 32.44; H, 6.87; N, 7.50%.

2.3. X-ray crystallography

A suitable single-crystal of **1–5** was carefully selected under a polarizing microscope. *Data collection*: Bruker Apex2 AXS CCD diffractometer, Mo Kα radiation (λ = 0.71073 Å), graphite monochromator, ω-scans, temperature 203(2) K. *Data collection* with APEX2 [22], respectively, cell refinement and data reduction with SAINT [22], experimental absorption correction with SADABS [23]. *Structure analysis and refinement*: the structures were solved by direct methods (SHELXS-97); refinement was done by full-matrix least squares on F^2 using the SHELXL-97 program suite [24]. All non-hydrogen positions were refined with anisotropic displacement parameters. Hydrogen atoms on carbon were positioned geometrically (C–H = 0.99 Å for aliphatic CH, C–H = 0.98 Å for CH_2) and refined using a riding model (AFIX 13 and 23 respectively), with U_{iso}(H) = 1.2U_{eq}(C). Protic H atoms on the crystal water (in **1**), the C–OH, NH_3^+ and $-PO_3H^-$ groups were found and refined with U_{iso}(H) = 1.5U_{eq}(O), except for the structure of **2** where these H atoms were positioned geometrically (O–H = 0.83 Å, N–H = 0.90 Å) and refined using a riding model (AFIX 83 for –OH, 133 for $-NH_3$), with U_{iso}(H) = 1.5U_{eq}(O/N). The refinement of the structure of **2** found two remaining residual electron density peaks of about 2 e Å^{-3}, each, at a distance of 1.6 and 1.5 Å to N1 and N2, respectively. This was suggestive of a partial oxidation of the N atoms to a hydroxylamine; however, further refinement of such a less than 10% crystal impurity was not possible. The representative nature of the single crystals investigated was verified by positively matching the measured. X-ray powder diffractogram of a larger crystal selection with the diffractogram simulated from the data of the single-crystal X-ray refinement (see Figs. S1–S4 in Supplementary data).

Crystal data and details on the structure refinement are given in Table 1. Graphics were drawn with DIAMOND [25].

3. Results and discussion

Hydrothermal reactions of the metal dichlorides of iron, copper and zinc with the sodium salts of 5-ammonium-1-hydroxypentylidene-1, 1-bisphosphonate, $Na_2HAC_5OHP_2$ or 3-ammonium-1-hydroxypropy-

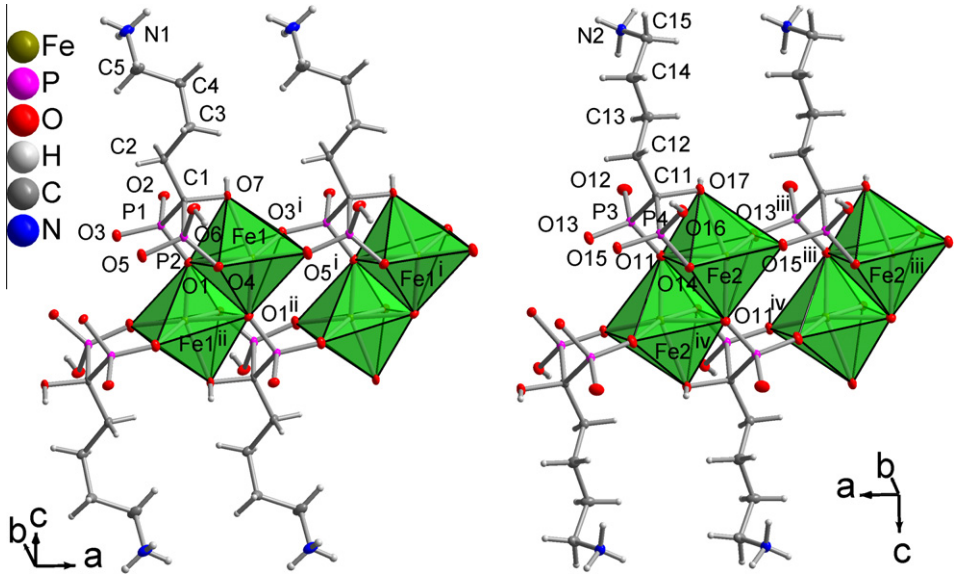

Fig. 1. Thermal ellipsoid plots (50%) of the two symmetry independent iron–bisphosphonate coordination spheres and strands in **1** with polyhedral representation around iron; selected distances and angles in Table 2 and Table S2, Supplementary data. (For the graphic in color, the reader is referred to the web version of this article.)

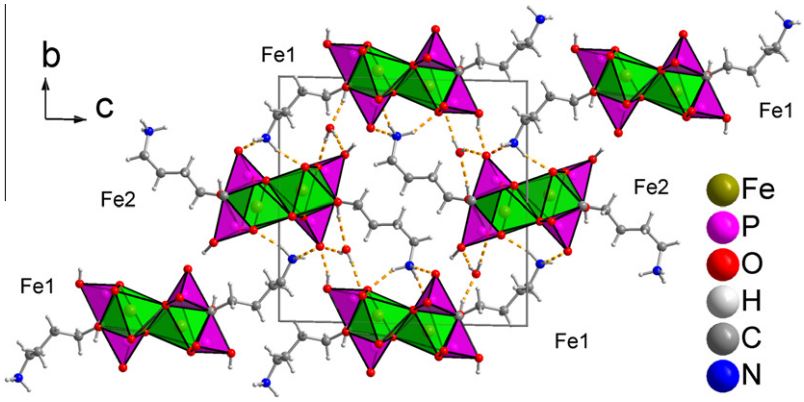

Fig. 2. Packing diagram for **1** with the crystal water molecule; projection on the *ab* plane and view along the strands in the *a* direction; polyhedral representation around the Fe and P atoms; the inter-strand hydrogen bonds are shown as dashed (orange) lines; see Fig. S5 and Table S1 for hydrogen-bonding details. (For the graphic in color, the reader is referred to the web version of this article.)

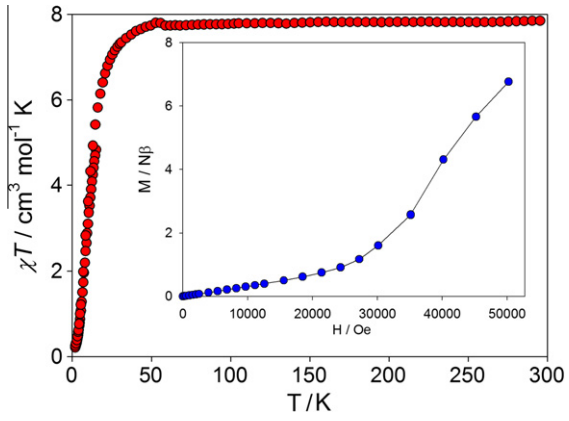

Fig. 3. Thermal dependence of the $\chi_M T$ product (•) for **1**. The inset shows the magnetization vs. *H* plot at 2 K (•). (For the graphic in color, the reader is referred to the web version of this article.)

Table 2
Selected bond distances (Å) and angles (°) in **1**[a].

Fe1		Fe2	
Fe1–O1	2.333(2)	Fe2–O11	2.3507(19)
Fe1–O1^{ii}	2.0481(18)	Fe2–O11^{iv}	2.0961(18)
Fe1–O3^{i}	2.0950(18)	Fe2–O13^{iii}	1.980(2)
Fe1–O4	2.1608(18)	Fe2–O14	2.059(2)
Fe1–O5^{i}	2.099(2)	Fe2–O15^{iii}	2.1819(18)
Fe1–O7	2.202(2)	Fe2–O17	2.324(2)
Fe1–O1–Fe1^{ii}	105.89(8)	Fe2–O11–Fe2^{iv}	93.65(7)

[a] Corresponding Fe–O distances are placed side by side. Symmetry transformations: i = 1 + *x*, *y*, *z*; ii = 1 − *x*, −*y*, 1 − *z*; iii = −1 + *x*, *y*, *z*; iv = −*x*, 1 − *y*, 2 − *z*. Additional O–Fe–O angles are given in Table S2, Supplementary data.

lidene-1,1-bisphosphonate (pamidronate), NaH_2PAM yield the metal ammonium-1-hydroxyalkylidene-diphosphonates **1–4** in good yield. From the reaction of $NiCl_2$ with $Na_2HAC_5OHP_2$ the 5-ammonium-1-hydroxypentylidene-1-phosphonic acid zwitterion,

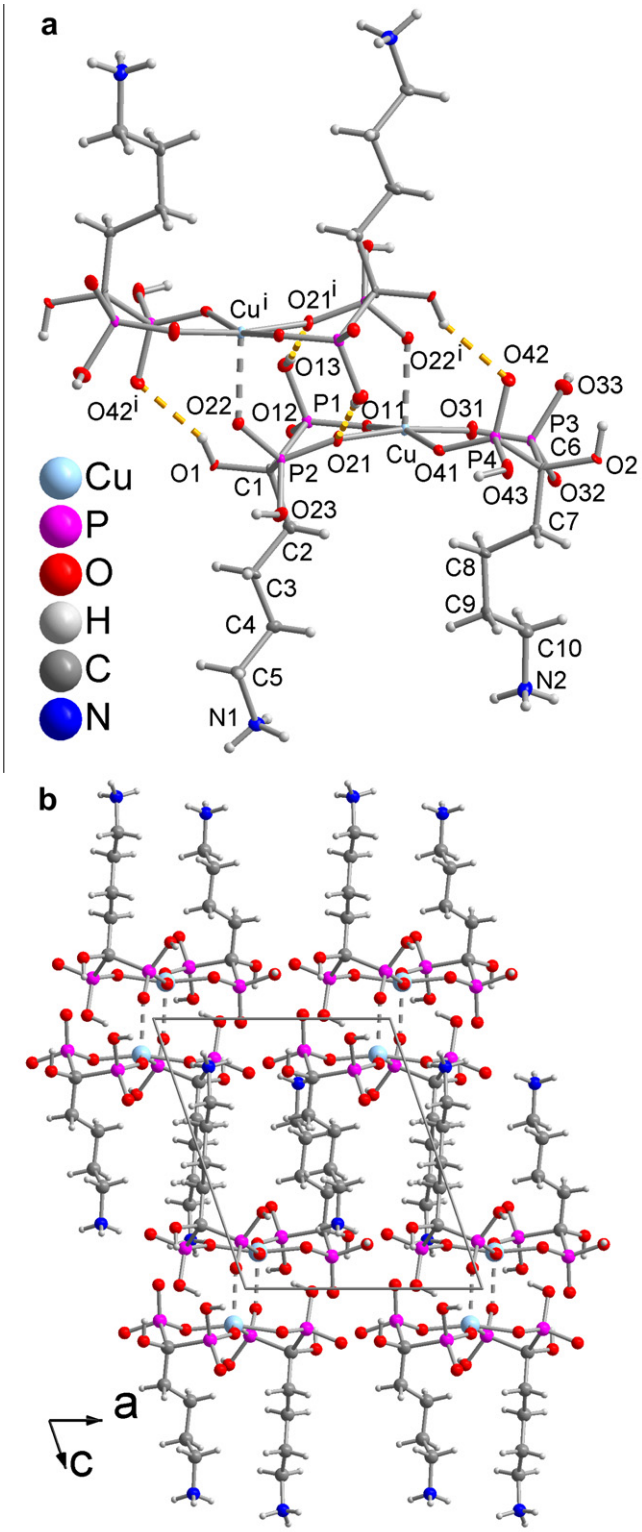

Fig. 4. (a) Thermal ellipsoid plot (50%) of a dimeric molecular pair in the copper compound **2** with the intra-dimer hydrogen bonds (dashed orange lines) and (b) packing diagram of **2** projected onto the *ac* plane; dashed grey lines indicate the long apical Cu···O bonds which connect the two halves of the dimer; selected distances Cu–O11 1.954(5), Cu–O21 1.965(5), Cu–O31 1.964(5), Cu–O41 1.933(5), Cu–O22^{i} 2.292(5); selected angles in Table S3; see Fig. S6 and Table S4 for hydrogen-bonding details; symmetry transformation i = 2 − *x*, −*y*, −*z*. (For the graphic in color, the reader is referred to the web version of this article.)

$^{+}H_3N(CH_2)_4CH(OH)PO_3H^{-}$, **5** was obtained as a result of P–C bond hydrolysis (Scheme 1).

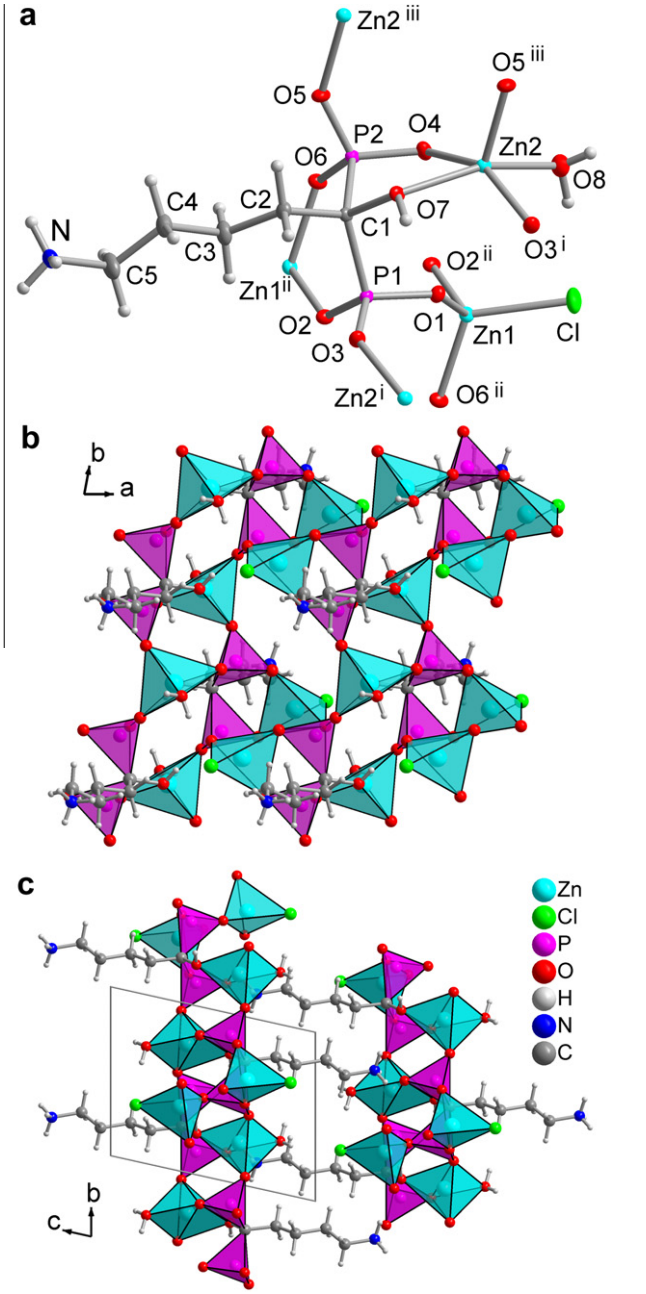

Fig. 5. (a) Thermal ellipsoid plot (50%) of the formula unit and zinc coordination sphere in **3**; selected distances and angles in Table 3 and S5; (b) section of a layer in **3** with polyhedral representation around the Zn and P atoms; (c) layer arrangement in **3** along *c*. The inter-layer hydrogen-bonding is not shown for clarity but noted in Table S6, Supplementary data. (For the graphic in color, the reader is referred to the web version of this article.)

The structures of **1–5** contain the ammonium-(bis-)phosphonate in its zwitterionic form. For pamidronate this was also the case in the of the free zwitterionic acid, H_3PAM [26,27], the sodium monohydrate, $Na^{+}H_2PAM^{-}\cdot H_2O$ [16], the disodium pentahydrate, $2Na^{+}HPAM^{2-}\cdot 5H_2O$ [14], the calcium dihydrate, 1D-$[Ca(H_2PAM)_2]\cdot 2H_2O$ [15], the molecular zinc aqua complex, $[Zn(H_2PAM)_2(H_2O)_2]$ [28] and the two-dimensional iron network 2D-$[Fe(H_2PAM)_2]$ [18].

The structure of the Fe^{2+} compound 1D-{$[Fe(\mu_3\text{-}HA\text{-}C_5OHP_2)]\cdot H_2O$}, **1** contains two symmetry independent iron atoms and bisphosphonate ligands, each (Fig. 1). Both iron atoms and ligands show the identical coordination behavior. The iron coordination polyhedra are distorted octahedra from five oxygen atoms of

bridging phosphonate groups and a sixth hydroxypentylidene donor. Each bisphosphonate ligand bridges between three iron atoms. Two inversion symmetry-related Fe atoms form an edge-sharing bi-octahedral repeat or secondary building unit which is extended into strands along the *a* direction through the bisphosphonate bridging action (Fig. 1). The hydroxy-O and two phosphonate-O atoms cover one octahedral face with one of the phosphonate-O atoms also bridging between the Fe atoms in the dinuclear unit. With the remaining O atoms the bisphosphonate ligand bridges to the adjacent dinuclear unit in a chelating action. Two of the seven oxygen atoms of the bisphosphonate ligand, including the P–OH group are not utilized in metal coordination but participate in the hydrogen-bonding network (Fig. S5, Supplementary data).

There are differences in the corresponding Fe–O distances and O–Fe–O angles in **1** but the major apparent difference for the two symmetry independent Fe(μ_3-HAC_5OHP_2) units lies in the pentylidene conformations: For the Fe1(P1–P2) unit the C2–C3–C4–C5 conformation is cisoid with a torsion angle of 68.2(3)°, for the Fe2(P3–P4) unit the torsion angle for the transoid C12–C13–C14–C15 conformation is 173.5(2)° (Fig. 1).

The two symmetry independent iron–bisphosphonate strands run parallel along the *a* direction in **1**. Neighboring strands are organized through the Coulomb attraction between the positive ammonium group and the negative phosphonate groups, supported by hydrogen-bonding. One crystal water molecule per formula unit is included in the hydrogen-bonding network. All protic N–H and P/C–OH hydrogen atoms in **1** are involved in hydrogen-bonding (Fig. 2 and S5 and Table S1, Supplementary data). The hydrogen bonds are charge-assisted, that is, the hydrogen bond donor and/or acceptor carry positive and negative ionic charges, respectively, hence are rather strong and short, in the case of $-NH_3^+\cdots{}^-O-P$, $-P-OH\cdots{}^-O-P$ and $-C-OH\cdots{}^-O-P$ [29].

The 1:1 Fe:ligand ratio requires a dinegative $^+H_3N(CH_2)_4C(OH)(PO_3^{2-})(PO_3H^-)$ ligand with only one proton left on one phosphonate arm for Fe^{2+}. Bond valence sum calculations [30–33] for the iron atoms in **1** based on the Fe–O distances of the single-crystal structure analysis give a value of 1.974 or 2.112 for Fe1 (as Fe(II) or Fe(III), respectively) and of 1.995 or 2.135 for Fe2 (as Fe^{III} or Fe^{II}). This suggests Fe1 and Fe2 to be in the +II oxidation state. Since the occupation factors of any protic hydrogen atoms and the Fe oxidation states are closely related [34,35], the single-crystal X-ray structure refinement alone may lead to an ambiguous formula assignment. The Fe(II) oxidation state was experimentally determined from a quantitative polarographic Fe(II)/Fe(III) speciation analysis [20] (see Section 2).

The temperature dependence of the $\chi_M T$ product for compound **1** is shown in Fig. 3 [χ_M corresponds to the molar magnetic susceptibility per two iron(II) ions]. The $\chi_M T$ product at room temperature has a value of 7.8 $cm^3\ mol^{-1}\ K$ and it remains practically constant down to 50 K. In this temperature range compound **1** follows the Curie law and the values calculated for *g* and *S* correspond to the expected ones for high-spin iron(II) complexes ($g = 2.28$ and $S = 2$, $\chi_M T = N\beta^2 g^2 S(S+1)/3kT$) [36–39]. At lower temperatures $\chi_M T$ continuously decreases reaching a value of 0.25 $cm^3\ mol^{-1}\ K$ at 2 K. This behavior is indicative of the occurrence of a dominant antiferromagnetic coupling in **1** at low temperatures. The antiferromagnetic coupling is supported by the field dependence of the magnetization plot, in which compound **1** displays a metamagnetic behavior (insert of Fig. 3).

The structure of **1** consists of μ-phosphate-O-bridged iron(II) dimers that are linked by phosphate groups to yield strands or double-chains running in the *a* direction (Fig. 1). The magnetic coupling through the phosphate groups is expected to be very weak, thus, the antiferromagnetic coupling takes place mainly through the intra-dimer (bi-octahedral) Fe–O–Fe magnetic exchange-pathway with angles of 105.89° and 93.65° (Table 2). Antiferromagnetic behavior has been also observed in other phosphate and μ-oxo-bridged iron(II) complexes [40] and in 1D-$[Co(II)\{CH_3C(OH)(PO_3)(PO_3H)\}]^{2-}$ chains [8d]. The magnetic study performed on **1** also supports the iron(II) oxidation state.

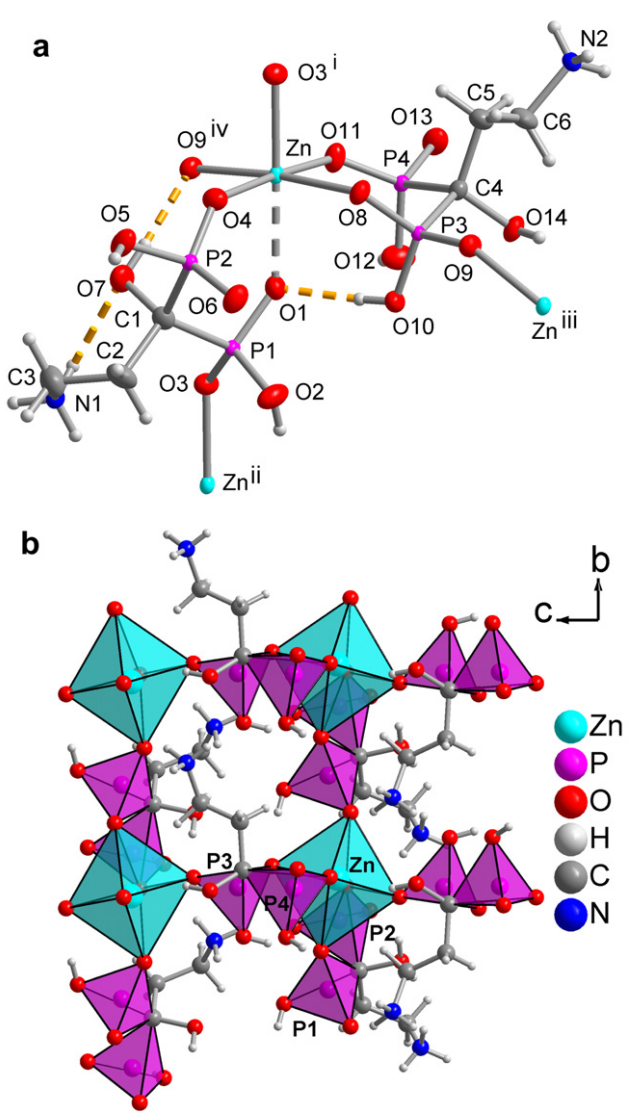

Fig. 6. (a) Thermal ellipsoid plot (50%) of the formula unit and zinc coordination sphere in **4**, showing also the two intra-layer H-bonds (dashed orange lines); (b) section of a layer in **4** with polyhedral representation around the Zn and P atoms; selected distances and angles in Table 3 and S5; hydrogen bonds in Table S7, Supplementary data. (For the graphic in color, the reader is referred to the web version of this article.)

Table 3
Selected bond distances (Å) in **3** and **4**[a].

	3		**4**
Zn1–Cl	2.2672(6)	Zn–O1	2.3440(17)
Zn1–O1	1.9474(14)	Zn–O3^{i}	2.1203(17)
Zn1–O2^{ii}	1.9349(15)	Zn–O4	2.0163(17)
Zn1–O6^{ii}	1.9626(13)	Zn–O8	2.0826(18)
Zn2–O3^{i}	1.9879(15)	Zn–O9^{iv}	2.0601(18)
Zn2–O4	2.0055(15)	Zn–O11	2.0821(17)
Zn2–O5^{iii}	1.9514(14)		
Zn2–O7	2.1428(14)		
Zn2–O8	2.0979(16)		

[a] Selected angles in Table S5 for **3** and **4**; symmetry transformations: In **3**: i = $-x$, $1-y$, $1-z$; ii = $1-x$, $1-y$, $1-z$; iii = $-x$, $2-y$, $1-z$. In **4**: i = x, $1+y$, z; iv = x, $-y$, $-0.5+z$.

The copper compound [Cu($H_2AC_5OHP_2$)$_2$], **2** is a molecular complex. Two mono-deprotonated, uni-negative bisphosphonate ligands coordinate the Cu^{2+} atom in the square plane. Two such complexes assemble into a dimer through the mutual bridging action of one deprotonated P–O atom along the Jahn–Teller distorted long apical bond and supported by hydrogen bonds (Fig. 4).

The ammonium-pentylidene tails separate the structure of **2** into hydrophilic layers containing the Cu{C(OH)(POH_3)$_2$} and {NH_3} units and into hydrophobic layers with the alkyl {CH_2–CH_2–CH_2–CH_2} chain (Fig. 4b). All protic N–H and P/C–OH hydrogen atoms in **2** are involved in charge-assisted [29] hydrogen-bonding (Fig. 4a and S6 and Table S4, Supplementary data).

The crystal structure of the zinc compound 2D-{[Zn_2(μ_5-AC_5OHP_2)Cl], **3** contains two crystallographically different zinc atoms. The atom Zn1 is tetrahedrally coordinated by a chlorine atom and three oxygen atoms from bridging phosphonate groups, with two also acting as a chelating bisphosphonate ligand. Atom Zn_2 is five-fold (square pyramidal, $\tau = 0.17$ [41]) coordinated by oxygen atoms from an aqua ligand, a hydroxypentylidene-phosphonate chelate and two bridging phosphonate groups (Fig. 5a). No proton is left on either of the $-PO_3^{2-}$ groups of the crystallographically unique, triply negative ammonium–bisphosphonate ligand. The bisphosphonate ligand bridges between five zinc atoms, thereby utilizing all of its seven oxygen atoms in metal coordination (Fig. 5a).

The bridging action of the bisphosphonate ligand in **3** gives rise to a 2D layer structure where each {PO_3C} tetrahedron links two {$ZnClO_3$} tetrahedra and one {ZnO_5} square-pyramid (Fig. 5b). These layers run parallel to the *ab* plane. Adjacent layers are organized through the Coulomb attraction between the positive ammonium group and the negative phosphonate group, supported by charge-assisted hydrogen-bonding (Table S6) [29]. The ammonium-pentylidene groups keep the layers apart (Fig. 5c). As seen before in the structure of **1** and **2** the alkyl chains act as separators between the hydrophilic layers with the polar Zn{C(OH)(POH_3)$_2$}, {Cl} and {NH_3} units.

The zinc structure 2D-{[Zn(μ-H_2PAM)$_2$], **4** contains one crystallographically independent zinc atom and two uni-negative bisphosphonate ligands. The zinc atom in this pamidronate compound **4** is distorted-octahedrally coordinated by six oxygen atoms, four from chelating bisphosphonate ligands and two from bridging phosphonate groups (Fig. 6a). One of the six Zn–O bonds is slightly elongated (2.344 Å versus 2.016–2.120 Å) (Table 3). One $-PO_3H^-$ group of the two crystallographically different bisphosphonate ligands is bridging between two zinc atoms, the other is only terminally coordinated to a metal atom. Only three out of the seven bisphosphonate oxygen atoms and none of the P/C–OH groups are involved in metal coordination. The zinc-pamidronate compound **4** is isostructural to the Fe^{2+} salt of pamidronate, 2D-{[Fe(μ-H_2PAM)$_2$] [18]. In retrospective this isostructural character confirmed the Mössbauer-based Fe^{2+} charge assignment and the full protic hydrogen occupation (1.0) of the two hydrogenophosphonato and ammonium groups with a single negative charge for each pamidronate ligand [18].

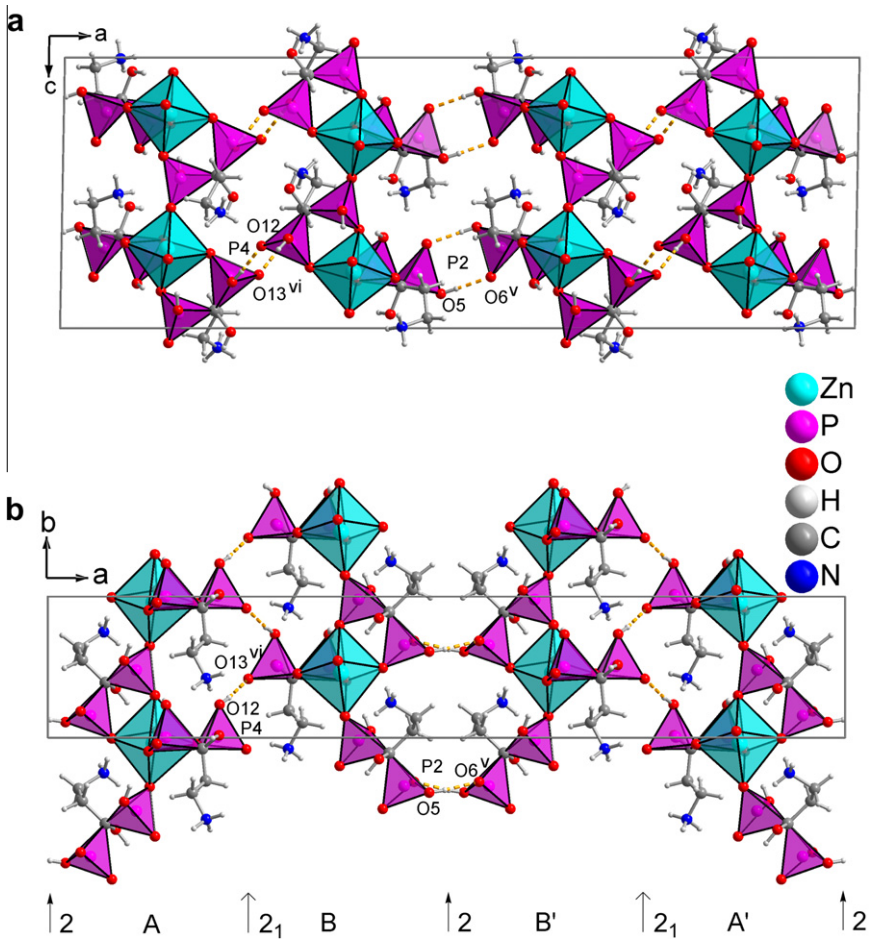

Fig. 7. Layer arrangement in **4** along *a* projected onto the (a) *ac* and (b) *ab* plane. The axes of rotation in (b) indicate the symmetry relationships between the layers (2 = two-fold proper axis of rotation, 2_1 = two-fold screw axis). Due to their different orientation the layers form an ABB′A′ sequence. The strong inter-layer head-to-tail hydrogen-bonding between the phosphonate groups is indicated as dashed orange lines. Additional hydrogen-bonding from the NH_3^+ groups is not shown for clarity; see Table S7 for hydrogen-bonding details. (For the graphic in color, the reader is referred to the web version of this article.)

The crystal structure of the zinc compound **4** is built from layers of alternating corner-sharing $\{ZnO_6\}$ octahedra and $\{PO_3C\}$ tetrahedra (Fig. 6b). These layers run parallel to the *bc* plane and are connected by hydrogen bonds along the *a* direction (Fig. 7). The hydrogen-bonding interaction to each side of the layer is different and creates a sequence of layers which can be described as ABB′A′. The relationship between B–B′ and A-A′ is by a two-fold rotation axis (2) parallel to *b* at (0 or 1/2, *y*, 1/4 or 3/4). Layers A–B or B′–A′ are related by a two-fold screw axis (2_1) parallel to *b* at (1/4 or 3/4, *y*, 1/4 or 3/4). Different from the structures of **1–3** it is not the Coulomb attraction between the positive ammonium group and the negative phosphonate groups which organizes the inter-layer arrangement. The propylidene chain in the pamidronate ligand is apparently too short. Thus, the ammonium group is oriented within the same layer. The inter-layer arrangement is primarily due to strong head-to-tail charge-assisted [29] hydrogen bonds between the phosphonate groups. The hydrogen-bonding from the non-bridging phosphonate groups of P2 between B and B′ (or A and A′) is the well-known complementary $R_2^2(8)$ graph-set motif [42], akin to the head-to-tail carboxylic acid–acid interaction, between two symmetry-related $-PO_2(OH)$-groups (Fig. 7a). This is different from the H-bonds between A and B (or B′ and A′). There, between A and B (or B′ and A′) the non-bridging phosphonate groups of P4 are oriented towards each other. Here the hydrogen-bonding between the $PO_2(OH)$-groups is not complementary but a C(4) chain graph-set motif [42] along *b* (Fig. 7b).

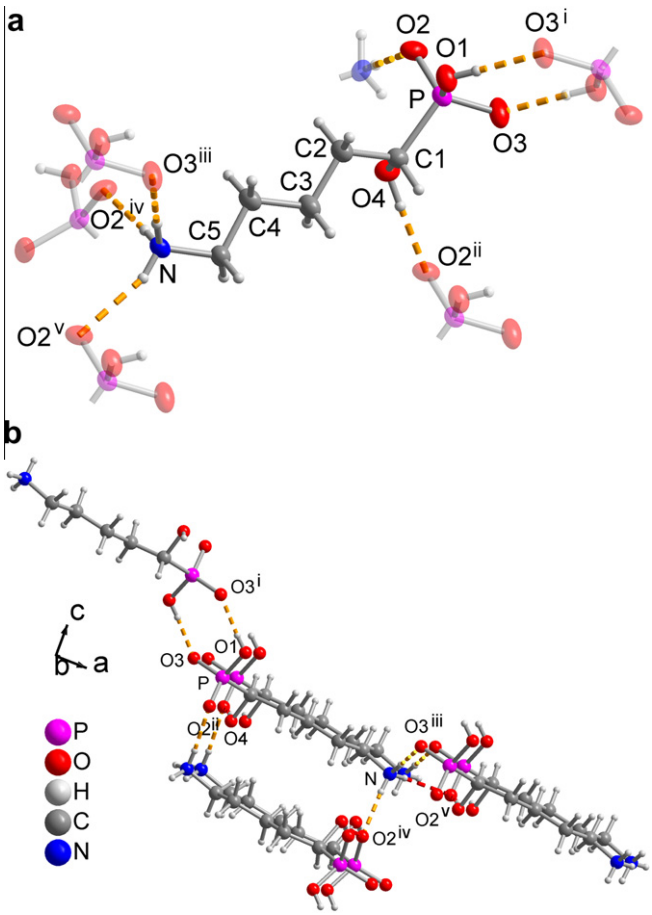

Fig. 8. (a) Thermal ellipsoid plot (50%) of the zwitterion **5**, showing also its surrounding H-bonds (dashed orange lines); (b) section of the packing diagram of the zwitterion **5** with the 3D hydrogen-bonding network; for details see Table 4. Selected non-hydrogen distances (Å) and angles (°): P–O1 1.5635(15), P–O2 1.5036(15), P–O3 1.5201(14), P–C1 1.809(2), O2–P–O3 112.84(9), O2–P–O1 110.66(9), O3–P–O1 110.88(8), O1–P–C1 104.96(9), O2–P–C1 109.08(9), O3–P–C1 108.06(9). (For the graphic in color, the reader is referred to the web version of this article.)

Table 4
Hydrogen-bonding interactions in **5**.

D–H···A[a]	D–H (Å)	H···A (Å)	D···A (Å)	D–H···A (°)
O1–H01···O3^{i}	0.76(3)	1.76(3)	2.525(2)	176(3)
O4–H4···O2^{ii}	0.91(3)	1.75(3)	2.651(2)	169(3)
N–H1···O3^{iii}	0.95(3)	1.85(3)	2.799(2)	179(2)
N–H2···O2^{iv}	0.83(3)	1.97(3)	2.796(2)	177(2)
N–H3···O2^{v}	0.84(3)	2.13(3)	2.941(2)	160(2)

[a] D = donor, A = acceptor. For found and refined atoms the standard deviations are given. Symmetry transformation: i = −*x*, −*y*, 1 − *z*; ii = *x*, 1 + *y*, *z*; iii 1 + *x*, *y*, *z*; iv = 1 − *x*, 0.5 + *y*, 0.5 − *z*; v = 1 + *x*, 1 + *y*, *z*.

The crystal structure of compound **5** contains the 5-ammonium-1-hydroxypentylidene-1-phosphonate zwitterion as part of a three-dimensional hydrogen-bonding network (Fig. 8). Each protic H atom on the C–OH, NH_3^+ and $-PO_3H^-$ group forms a charge-assisted [29] hydrogen bond to the $P–O^{(-)}$ atoms O2 or O3, respectively. The O2 atom accepts three H-bonds, the O3 atom two of them (Table 4). The $-PO_3H^-$ group forms a strong head-to-tail hydrogen bond or complementary $R_2^2(8)$ graph-set motif [42] to an inversion symmetry-related phosphonate group (O1–H01···O3^{i}) [3b,43].

4. Conclusions

The iron and zinc compounds 1D-{$[Fe(\mu_3\text{-}\eta^5\text{-}HAC_5OHP_2)]\cdot H_2O$}, **1**, 2D-{$[Zn_2(\mu_5\text{-}\eta^7\text{-}AC_5OHP_2)Cl]$}, **3**, and 2D-{$[Zn(\mu_2\text{-}\eta^3\text{-}H_2PAM)_2]$}, **4**, obtained upon hydrothermal synthesis are infinite metal–ligand networks of one- or two-dimensionality where the bisphosphonate ligands bridge (μ_n) between *n* metal atoms by utilizing between three to seven oxygen donor atoms for metal coordination (η^3–η^7) including the hydroxyl oxygen atom (C–OH) in **1** and **3**. Higher dimensionalities were observed in 3D-$[Fe(II)\{HO_3P(CH_2)_2PO_3\}(H_2O)]$ [9b], 3D-$[Pb_2\{HN(CH_2PO_3)_2\}]\cdot 2H_2O$ [3d], 3D-$[Zn_3\{CH_3N(CH_2PO_3H)_2\}]$ [44]. The copper compound $[Cu(\eta^2\text{-}H_2AC_5OHP_2)_2]$, **2**, is a molecular complex. The zwitterionic nature of the now bis- or tetrakis-deprotonated ammonium–bisphosphonate ligands is retained in the metal complexes. Hydrogen-bonding which is charge-assisted [29] in the case of $-NH_3^+\cdots{}^-O–P$, $–P–OH\cdots{}^-O–P$ and $–C–OH\cdots{}^-O–P$ extends the metal–ligand structures to a three-dimensional supramolecular network in **1–4**, similar to the metal bisphosphonate structures reported in, for example, [3c,8g,11b,44,45]. The Fe(II) oxidation state in **1** is verified from bond valence sum calculations, a quantitative polarographic Fe(II)/Fe(III) speciation analysis as well as a temperature variable magnetic study.

Acknowledgments

We thank the DFG for financial support through Grant Ja466/14-1/2 and through Grant Ja466/16-1 for KAS, collaboration with Jordan.

Appendix A. Supplementary data

CCDC 764562, 764563, 764564, 764565 and 764566 contain the supplementary crystallographic data for **1–5**. These data can be obtained free of charge via http://www.ccdc.cam.ac.uk/conts/retrieving.html, or from the Cambridge Crystallographic Data Centre, 12 Union Road, Cambridge CB2 1EZ, UK; fax: (+44) 1223-336-033; or e-mail: deposit@ccdc.cam.ac.uk. Supplementary data associated

with this article can be found, in the online version, at doi:10.1016/j.poly.2010.05.025.

References

[1] (a) K. Maeda, Micropor. Mesopor. Mater. 73 (2004) 47;
(b) A. Clearfield, Z. Wang, J. Chem. Soc., Dalton Trans. (2002) 2937;
(c) A. Clearfield, Curr. Opin. Solid State Mater. Sci. 6 (2002) 495.

[2] (a) M. Kontturi, S. Kunnas-Hiltunen, J.J. Vepsäläinen, M. Ahlgrén, Solid State Sci. 8 (2006) 1098;
(b) G. Alberti, U. Constantino, M. Casciola, R. Vivani, Adv. Mater. 8 (1996) 291.

[3] (a) J. Liang, G.K.H. Shimizu, Inorg. Chem. 46 (2007) 10449;
(b) R. Clarke, K. Latham, C. Rix, M. Hobday, J. White, CrystEngComm 7 (2005) 28;
(c) S. Midollini, A. Orlandini, A. Vacca, Inorg. Chem. Commun. 7 (2004) 1113;
(d) B.-P. Yang, Z.-M. Sun, J.-G. Mao, Inorg. Chim. Acta 357 (2004) 1583;
(e) M. Riou-Cavellec, M. Sanselme, G. Férey, J. Mater. Chem. 10 (2000) 745.

[4] (a) G. Cao, H.-G. Hong, T.E. Mallouk, Acc. Chem. Res. 25 (1992) 420;
(b) J.W. Johnson, J.F. Brody, R.M. Alexander, B. Pilarski, A.R. Katritzky, Chem. Mater. 2 (1990) 198 (Molecular recognition).

[5] C. Janiak, Dalton Trans. (2003) 2781.

[6] J.L. Snover, H. Byrd, E.P. Suponeva, E. Vicenzi, M.E. Thompson, Chem. Mater. 8 (1996) 1490.

[7] T. Rojo, J.L. Mesa, J. Lago, B. Bazan, J.L. Pizarro, M.I. Arriortua, J. Mater. Chem. 19 (2009) 3793 (Review).

[8] (a) S.-Z. Hou, D.-K. Cao, X.-G. Liu, Y.-Z. Li, Li-Min Zheng, Dalton Trans. (2009) 2746;
(b) Y.S. Ma, Y. Song, L.M. Zheng, Inorg. Chim. Acta 361 (2008) 1363;
(c) Z.-C. Zhang, S. Gao, L.-M. Zheng, Dalton Trans. (2007) 4681;
(d) L.-M. Zheng, S. Gao, P. Yin, X.-Q. Xin, Inorg. Chem. 43 (2004) 2151;
(e) P. Yin, S. Gao, L.-M. Zheng, X.-Q. Xin, Chem. Mater. 15 (2003) 3233;
(f) P. Yin, S. Gao, L.-M. Zheng, Z.-M. Wang, X.-Q. Xin, Chem. Commun. (2003) 1076;
(g) P. Yin, X.-C. Wang, S. Gao, L.-M. Zheng, J. Solid State Chem. 178 (2005) 1049 (Cobalt compounds).

[9] (a) Y. Lalatonne, C. Paris, J.M. Serfaty, P. Weinmann, M. Lecouvey, L. Motte, Chem. Commun. (2008) 2553;
(b) C.A. Merrill, A.K. Cheetham, Inorg. Chem. 44 (2005) 5273;
(c) H.-H. Song, L.-M. Zheng, G.-S. Zhu, Z. Shi, S.-H. Feng, S. Gao, Z. Hu, X.-Q. Xin, J. Solid State Chem. 164 (2002) 367;
(d) M. Riou-Cavellec, C. Serre, J. Robino, M. Noguès, J.-M. Grenèche, G. Férey, J. Solid State Chem. 147 (1999) 122;
(e) L.-M. Zheng, H.-H. Song, C.-H. Lin, S.-L. Wang, Z. Hu, Z. Yu, X.-Q. Xin, Inorg. Chem. 38 (1999) 4618;
(f) A.W. Herlinger, J.R. Ferraro, J.A. Garcia, R. Chiarizia, Polyhedron 17 (1998) 1471 (Iron compounds).

[10] (a) B. Zurowska, A. Brzuszkiewicz, J. Ochocki, Polyhedron 27 (2008) 1721;
(b) Y.S. Ma, T.W. Wang, Y.Z. Li, L.M. Zheng, Inorg. Chim. Acta 361 (2008) 4117;
(c) D.-K. Cao, X.-J. Xie, Y.-Z. Li, L.-M. Zheng, Dalton Trans. (2008) 5008;
(d) E. Spodine, D. Venegas-Yazigi, S. Ushak, V. Paredes-Garcia, M. Saldias, E. Le Fur, J.Y. Pivan, Polyhedron 26 (2007) 2121;
(e) J. Le Bideau, C. Payen, P. Palvadeau, B. Bujoli, Inorg. Chem. 33 (1994) 4885 (Copper compounds).

[11] (a) M. Menelaou, M. Dakanali, C.P. Raptopoulou, C. Drouza, N. Lalioti, A. Salifoglou, Polyhedron 28 (2009) 3331;
(b) S. Kunnas-Hiltunen, M. Matilainen, J.J. Vepsäläinen, M. Ahlgrén, Polyhedron 28 (2009) 200;
(c) P.J. Byrne, D.S. Wragg, J.E. Warren, R.E. Morris, Dalton Trans. (2009) 795;
(d) C.Y. Fang, Z.X. Chen, X.F. Liu, Y.T. Yang, M.L. Deng, L.H. Weng, Y. Jia, Y.M. Zhou, Inorg. Chim. Acta 362 (2009) 2101;
(e) K. Latham, K.F. White, K.B. Szpakolski, C.J. Rix, J.M. White, Inorg. Chim. Acta 362 (2009) 1872;
(f) G. Yucesan, J.E. Valeich, H.X. Liu, W. Ouellette, C.J. O'Connor, J. Zubieta, Inorg. Chim. Acta 362 (2009) 1831;
(g) J. Galezowska, P. Kafarski, H. Kozlowski, P. Mlynarz, V.M. Nurchi, T. Pivetta, Inorg. Chim. Acta 362 (2009) 707;
(h) Z.Y. Du, Y.R. Xie, H.R. Wen, Inorg. Chim. Acta 362 (2009) 351;
(i) S.M. Ying, X.F. Li, J.G. Huang, J.Y. Lin, W.T. Chen, G.P. Zhou, Inorg. Chim. Acta 361 (2008) 1547;
(j) D.R. Jansen, J.R. Zeevaart, Z.I. Kolar, K. Djanashvili, J.A. Peters, G.C. Krijger, Polyhedron 27 (2008) 1779;
(k) R. Murugavel, S. Shanmugan, Dalton Trans. (2008) 5358;
(l) V. Chandrasekhar, P. Sasikumar, R. Boomishankar, Dalton Trans. (2008) 5189 (Recent references).

[12] (a) W.R. Harris, C.E. Brook, C.D. Spilling, S. Elleppan, W. Peng, M. Xin, J. Van Wyk, J. Inorg. Biochem. 98 (2004) 1824;
(b) E. Gumienna-Kontecka, J. Galezowska, M. Drag, R. Latajka, P. Kafarski, H. Kozlowski, Inorg. Chim. Acta 357 (2004) 1632.

[13] (a) S. Mukherjee, C. Huang, F. Guerra, K. Wang, E. Oldfield, J. Am. Chem. Soc. 131 (2009) 8374;
(b) G. Duque, R. Segal, J. Bianco, J. Am. Geriatrics Soc. 53 (2005) 1633;
(c) T.J. Cho, I.H. Choi, Y.C. Chung, J. Pediatric Orthopaedics 25 (2005) 607;
(d) S.C.L.M. Cremers, S.E. Papapoulos, H. Gelderblom, J. Bone Miner. Res. 20 (2005) 1543;
(e) A.N. Toukap, G. Depresseux, J.P. Devogelaer, LUPUS 14 (2005) 517;
(f) J.M. Stephens, M.S. Aapro, M.F. Botteman, J. Clin. Oncol. 23 (Suppl. S) (2005) 44S (Part 1);
(g) J. Jung, G. Hwang, Y. Lee, J. Clin. Oncol. 23 (Suppl. S) (2005) 99S (Part 1).

[14] D. Vega, D. Fernández, J.A. Ellena, Acta Crystallogr., Sect. C 58 (2002) m77.

[15] D. Fernández, D. Vega, A. Goeta, Acta Crystallogr., Sect. C 58 (2002) m494.

[16] K. Stahl, S.P. Treppendahl, H. Preikschat, E. Fischer, Acta Crystallogr., Sect. E 61 (2005) m132.

[17] D.M. Black, P.D. Delmas, R. Eastell, I.R. Reid, S. Boonen, J.A. Cauley, F. Cosman, P. Lakatos, P.C. Leung, Z. Man, C. Mautalen, P. Mesenbrink, H. Hu, J. Caminis, K. Tong, T. Rosario-Jansen, J. Krasnow, T.F. Hue, D. Sellmeyer, E.F. Eriksen, S.R. Cummings, New Engl. J. Med. 356 (2007) 1809.

[18] K. Abu-Shandi, C. Janiak, Z. Naturforsch. B 60 (2005) 1250.

[19] K. Abu-Shandi, H. Winkler, C. Janiak, Z. Anorg. Allg. Chem. 632 (2006) 629.

[20] Metrohm Applikation 3-282-0599 "Speciation Fe(II)/Fe(III)", Metrohm Applikation 3-221-0291 and 3-245-0194 "Fe^{2+} and Fe^{3+} Determination Simultaneously".

[21] G.R. Kieczykowski, R.B. Jobson, D.G. Melillo, D.F. Reinhold, V.J. Grenda, I. Shinkai, J. Org. Chem. 60 (1995) 8310.

[22] APEX2 (Version 2.1-0) Data Collection Program for the CCD Area-Detector System, SAINT, Data Reduction and Frame Integration Program for the CCD Area-Detector System, Bruker Analytical X-ray Systems, Madison, Wisconsin, USA, 2006.

[23] G. Sheldrick, Program SADABS: Area-detector Absorption Correction, University of Göttingen, Germany, 1996.

[24] G.M. Sheldrick, Acta Crystallogr., Sect. A 64 (2008) 112.

[25] K. Brandenburg, DIAMOND (Version 3.2c), Crystal and Molecular Structure Visualization, Crystal Impact, K. Brandenburg & H. Putz Gbr, Bonn, Germany, 2009.

[26] L.M. Shkol'nikova, S.S. Sotman, E.G. Afonin, Kristallografiya 35 (1990) 1442.

[27] L.M. Shkol'nikova, S.S. Sotman, E.G. Afonin, Sov. Phys. Crystallogr. 35 (1990) 850.

[28] D. Fernández, G. Polla, D. Vega, J.A. Ellena, Acta Crystallogr., Sect. C 60 (2004) m73.

[29] (a) M.D. Ward, Chem. Commun. (2005) 5838. and references in this review;
(b) B.M. Drašković, G.A. Bogdanović, M.A. Neelakantan, A.-C. Chamayou, S. Thalamuthu, Y.S. Avadhut, J. Schmedt auf der Günne, S. Banerjee, C. Janiak, Cryst. Growth Des. 10 (2010) 1665;
(c) F. Zhuge, B. Wu, J. Liang, J. Yang, Y. Liu, C. Jia, C. Janiak, N. Tang, X.-J. Yang, Inorg. Chem. 48 (2009) 10249;
(d) E. Redel, C. Röhr, C. Janiak, Chem. Commun. (2009) 2103;
(e) E. Redel, M. Fiederle, C. Janiak, Z. Anorg. Allg. Chem. 635 (2009) 1139;
(f) B. Wu, J. Liang, J. Yang, C. Jia, X.-J. Yang, H. Zhang, N. Tang, C. Janiak, Chem. Commun. (2008) 1762;
(g) B. Wu, X. Huang, Y. Xia, X.-J. Yang, C. Janiak, CrystEngComm 9 (2007) 676;
(h) T. Dorn, A.-C. Chamayou, C. Janiak, New J. Chem. 30 (2006) 156;
(i) T. Dorn, C. Janiak, K. Abu-Shandi, CrystEngComm 7 (2005) 633.

[30] Bond valences (s) calculated from the bond lengths (R) according to $s = \exp(R_0 - R)/B$ and $R_0 = 1.734$ for Fe^{2+}–O, 1.759 for Fe^{3+}–O, B = 0.37. Program VALENCE (Version 2.00, February 1993) I.D. Brown, J. Appl. Crystallogr. 29 (1996) 479.

[31] I.D. Brown, R.D. Shannon, Acta Crystallogr., Sect. A 29 (1973) 266.

[32] I.D. Brown, K.K. Wu, Acta Crystallogr., Sect. B 32 (1976) 1957.

[33] I.D. Brown, D. Altermatt, Acta Crystallogr., Sect. B 41 (1985) 244.

[34] K. Abu-Shandi, H. Winkler, M. Gerdan, F. Emmerling, B. Wu, C. Janiak, Dalton Trans. (2003) 2815.

[35] K. Abu-Shandi, H. Winkler, B. Wu, C. Janiak, CrystEngComm 5 (2003) 180.

[36] O. Kahn, Molecular Magnetism, VCH, New York, 1993.

[37] M. Quesada, P. Hoog, P. Gamez, O. Roubeau, G. Aromí, B. Donnadieu, C. Massera, M. Lutz, A.L. Spek, J. Reedijk, Eur. J. Inorg. Chem. (2006) 1353.

[38] S. Konar, E. Zangrando, M.G.B. Drew, T. Mallah, J. Ribas, N.R. Chaudury, Inorg. Chem. 42 (2003) 5966.

[39] J.S. Sun, H. Zhao, X. Ouyang, R. Clérac, J.A. Smith, J.M. Clemente-Juan, C.J. Gómez-García, E. Coronado, K. Dunbar, Inorg. Chem. 38 (1999) 5841.

[40] W.L. Queen, S.J. Hwu, L. Wang, Angew. Chem., Int. Ed. 46 (2007) 5344.

[41] τ = (difference between the two largest angles)/60 for five-coordinated metal centers allows for the distinction between trigonal-bipyramidal (ideally τ = 1) and square-pyramidal (ideally τ = 0): A.W. Addison, T.N. Rao, J. Reedijk, J. van Rijnn, G.C. Verschoor, J. Chem. Soc., Dalton Trans. (1984) 1349.

[42] (a) M.C. Etter, Acc. Chem. Res. 23 (1990) 120;
(b) M.C. Etter, J.C. MacDonald, J. Bernstein, Acta Crystallogr., Sect. B 46 (1990) 256;
(c) M.C. Etter, J. Phys. Chem. 95 (1991) 4601.

[43] M. Lecouvey, C. Barbey, A. Navazza, A. Neuman, T. Prangé, Acta Crystallogr., Sect. C 58 (2002) o521.

[44] J.-G. Mao, Z. Wang, A. Clearfield, Inorg. Chem. 41 (2002) 2334.

[45] (a) L.-M. Zheng, P. Yin, X.-Q. Xin, Inorg. Chem. 41 (2002) 4084;
(b) A. Cabeza, X. Ouyang, C.V. Krishnamohan, M.A.G. Aranda, S. Bruque, A. Clearfield, Inorg. Chem. 41 (2002) 2325.